

Topological Lifshitz transition and novel edge states induced by non-Abelian SU(2) gauge field on bilayer honeycomb lattice

Wen-Xiang Guo(郭文祥) and Wu-Ming Liu(刘伍明)

Citation: Chin. Phys. B, 2022, 31 (**5**): 057302. DOI: 10.1088/1674-1056/ac3ecb
Journal homepage: http://cpb.iphy.ac.cn; http://iopscience.iop.org/cpb

What follows is a list of articles you may be interested in

Electronic structures and topological properties of $TeSe_2$ monolayers

Zhengyang Wan(万正阳), Hao Huan(郇昊), Hairui Bao(鲍海瑞), Xiaojuan Liu(刘晓娟), and Zhongqin Yang(杨中芹)

Chin. Phys. B, 2021, 30 (**11**): 117304. DOI: 10.1088/1674-1056/ac2489

Floquet topological phase transition in two-dimensional quadratic band crossing system

Guo-Bao Zhu(朱国宝) and Hui-Min Yang(杨慧敏)

Chin. Phys. B, 2021, 30 (**6**): 067304. DOI: 10.1088/1674-1056/abdda4

Progress on 2D topological insulators and potential applications in electronic devices

Yanhui Hou(侯延辉), Teng Zhang(张腾), Jiatao Sun(孙家涛), Liwei Liu(刘立巍), Yugui Yao(姚裕贵), Yeliang Wang(王业亮)

Chin. Phys. B, 2020, 29 (**9**): 097304. DOI: 10.1088/1674-1056/aba9c5

Topology of triple-point metals

Georg W. Winkler, Sobhit Singh, Alexey A. Soluyanov

Chin. Phys. B, 2019, 28 (**7**): 077303. DOI: 10.1088/1674-1056/28/7/077303

Quantum spin Hall and quantum valley Hall effects in trilayer graphene and their topological structures

Majeed Ur Rehman, A A Abid

Chin. Phys. B, 2017, 26 (**12**): 127304. DOI: 10.1088/1674-1056/26/12/127304

Topological Lifshitz transition and novel edge states induced by non-Abelian SU(2) gauge field on bilayer honeycomb lattice

Wen-Xiang Guo(郭文祥)[1,2] and Wu-Ming Liu(刘伍明)[1,2,3,†]

[1] *Beijing National Laboratory for Condensed Matter Physics, Institute of Physics, Chinese Academy of Sciences, Beijing* 100190, *China*
[2] *School of Physical Sciences, University of Chinese Academy of Sciences, Beijing* 100190, *China*
[3] *Songshan Lake Materials Laboratory, Dongguan* 523808, *China*

(Received 11 October 2021; revised manuscript received 25 November 2021; accepted manuscript online 1 December 2021)

We investigate the SU(2) gauge effects on bilayer honeycomb lattice thoroughly. We discover a topological Lifshitz transition induced by the non-Abelian gauge potential. Topological Lifshitz transitions are determined by topologies of Fermi surfaces in the momentum space. Fermi surface consists of $N = 8$ Dirac points at π-flux point instead of $N = 4$ in the trivial Abelian regimes. A local winding number is defined to classify the universality class of the gapless excitations. We also obtain the phase diagram of gauge fluxes by solving the secular equation. Furthermore, the novel edge states of biased bilayer nanoribbon with gauge fluxes are also investigated.

Keywords: topological Lifshitz transition, SU(2) gauge field, bilayer honeycomb lattice

PACS: 73.43.Nq, 64.70.Tg, 73.50.–h, 73.21.Ac **DOI:** 10.1088/1674-1056/ac3ecb

1. Introduction

In recent decades, the discovery of topological insulators has extended our understanding of topological states of matter tremendously.[1–3] In Landau theory of phase transitions, different states of matter are classified by spontaneous symmetry breaking. However, topological states cannot be distinguished from topological trivial states by symmetry, and thus topological phase transitions can not be characterized by a local order parameter.[1–3] Consequently, various topological invariants are introduced to identify the topological phase transitions.[1–3] Different from usual topological transitions, topological Lifshitz transitions[4–6] are determined by topologies of Fermi surfaces in momentum space. They are accompanied by the change of topology of Dirac points,[7] Weyl points,[8,9] nodal lines,[10,11] and so on.[5]

Since the first preparation of graphene,[12] two-dimensional materials have been investigated widely due to their various exotic properties and prospective applications. For instance, the charge carriers in graphene are massless Dirac fermions described by Dirac's relativistic equation,[13–15] which allows for the investigation of quantum electrodynamic phenomena. Furthermore, the Fermi surface of several Dirac points also makes graphene an excellent platform to study topological Lifshitz transitions.[4,5] However, owing to the inevitable disorder, defects, and impurities in materials, it is difficult for us to manipulate the materials arbitrarily. Fortunately, ultra-cold atoms in optical lattices[16,17] provide a flexible and controllable playground to stimulate the phenomena in condensed matter and particle physics, such as Mott transition[18–20] and gauge invariance.[21] Artificial gauge fields on neutral atoms have been created by atom–laser interaction,[22–27] which makes it possible to investigate the topological phase transitions in optical lattices.[28–42]

The SU(2) gauge effects on the honeycomb lattice have been investigated thoroughly.[30,31] The non-Abelian gauge potential induces an annihilation and creation of massless Dirac points. Different from the massless Dirac fermions in graphene, the charge carriers of bilayer graphene are massive chiral quasiparticles.[43,44] What's more, a tunable band gap has been realized by applying a biased electric field on bilayer graphene.[45–49] Accordingly, bilayer honeycomb lattice (BHL) has been studied widely and various exotic phenomena have been discovered.[50–59] Thus how the SU(2) gauge field will act on the BHL deserves to be investigated.

In this work, we investigate the SU(2) gauge effects on BHL. Based on the tight-binding model, we obtain the model with SU(2) gauge potential by Peierls substitution.[30,60,61] Then we discover a topological Lifshitz transition induced by the non-Abelian gauge potential by calculating the Fermi surfaces. The phase diagram of the gauge fluxes is also obtained by solving the secular equation. In addition, edge states of biased bilayer ribbons are studied under the influence of gauge potential.

The paper is organized as follows. In Section 2, we introduce the model. Then we analyze the topological Lifshitz transition induced by the non-Abelian SU(2) gauge potential in Section 3 and obtain the phase diagram of the transition in Section 4. Next in Section 5, the edge states of biased bilayer ribbon with gauge fluxes are studied. Finally, we summarize our results briefly in Section 6.

[†]Corresponding author. E-mail: wliu@iphy.ac.cn

© 2022 Chinese Physical Society and IOP Publishing Ltd

2. Tight-binding model with SU(2) gauge potential

The AB-Bernal stacking BHL, as shown in Figs. 1(a) and 1(b), is commonly described by a tight-binding Hamiltonian with the nearest-neighbor intra-layer hopping and the inter-layer hopping between A_1 and A_2 sites,[13–15,62–65]

$$H_{\rm t} = -t\sum_{\langle ij\rangle,l,\sigma} c^{\dagger}_{il\sigma}c_{jl\sigma} - t_{\perp}\sum_{i,l,\sigma} c^{\dagger}_{il\sigma}c_{i(1-l)\sigma}, \tag{1}$$

where t ($t_{\perp}$) is the intra-layer (inter-layer) hopping integral, i (j) and l denote the site and layer indices, respectively, and spin $\sigma = \uparrow,\downarrow$. $c^{\dagger}_{il\sigma}$ ($c_{il\sigma}$) is the creation (annihilation) operator. The Hamiltonian described in Eq. (1) corresponds to the optical lattice system of cold atoms. An experimental setup has been proposed to generate the Bernal stacking BHL through lasers.[52] For simplicity, we set $t = 1.0$ throughout the paper without loss of generality.

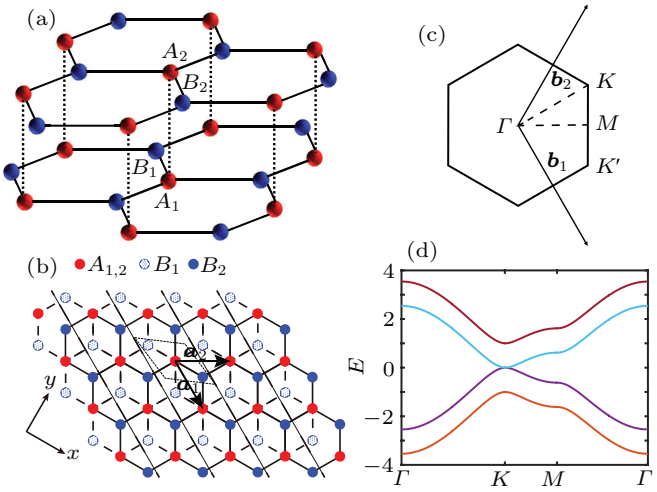


Fig. 1. (a) The illustration of the AB-Bernal stacking bilayer honeycomb lattice (BHL). (b) Top view of the BHL lattice. The cell consists of four sites, including A_1 (B_1) in the lower layer and A_2 (B_2) in the upper layer. The lattice primitive vectors $\boldsymbol{a}_1 = (\frac{3}{2}, -\frac{\sqrt{3}}{2})$, $\boldsymbol{a}_2 = (\frac{3}{2}, \frac{\sqrt{3}}{2})$. (c) The first Brillouin zone (FBZ) and the reciprocal lattice vector $\boldsymbol{b}_1 = \frac{2\pi}{3}(1, -\sqrt{3})$, $\boldsymbol{b}_2 = \frac{2\pi}{3}(1, \sqrt{3})$. $K = \frac{2\pi}{3}(1, \frac{1}{\sqrt{3}})$ and $K' = \frac{2\pi}{3}(1, -\frac{1}{\sqrt{3}})$ are two inequivalent corners of the FBZ. (d) The energy band structure for the Hamiltonian (2) along the loop $\Gamma \to K \to M \to \Gamma$ in the FBZ. One conduction band and one valence band touch parabolically at the K point no matter what $t_{\perp}$ equals to.

Under the basis $\{\psi_{B_1}, \psi_{A_1}, \psi_{A_2}, \psi_{B_2}\}$, the Hamiltonian (1) in the reciprocal space takes the form

$$H_{\rm t}(\boldsymbol{k}) = \begin{bmatrix} 0 & -tf(\boldsymbol{k}) & 0 & 0 \\ -tf^*(\boldsymbol{k}) & 0 & -t_{\perp} & 0 \\ 0 & -t_{\perp} & 0 & -tf(\boldsymbol{k}) \\ 0 & 0 & -tf^*(\boldsymbol{k}) & 0 \end{bmatrix}, \tag{2}$$

where $f(\boldsymbol{k}) = 1 + {\rm e}^{{\rm i}\boldsymbol{k}\cdot\boldsymbol{a}_1} + {\rm e}^{{\rm i}\boldsymbol{k}\cdot\boldsymbol{a}_2}$. The dispersion relations of the four energy bands [Fig. 1(d)] derived from the Hamiltonian (2) read as

$$\varepsilon(\boldsymbol{k}) = \frac{\pm\sqrt{t_{\perp}^2 + 4t^2|f(\boldsymbol{k})|^2} \pm t_{\perp}}{2}, \tag{3}$$

which is symmetric around the zero energy due to the electron–hole symmetry. We also find that $f(\boldsymbol{k}) = 0$ for two inequivalent corners of the first Brillouin zone (FBZ) [Fig. 1(c)], such that the lower conduction band and upper valence band touch at zero energy at the corners K and K'. We define $\boldsymbol{k} = \boldsymbol{K} + \boldsymbol{q}$ near the K point and expand the spectrum to investigate the low-energy properties. The low-energy band spectrum is approximately

$$\varepsilon_{\pm}(\boldsymbol{q}) = \pm\frac{9t^2|\boldsymbol{q}|^2}{4t_{\perp}} = \pm\frac{v_{\rm F}^2|\boldsymbol{q}|^2}{t_{\perp}}, \tag{4}$$

where $v_{\rm F} = 3t/2$ is the Fermi velocity of monolayer graphene.[13] The quasiparticles of the BHL model at low energies have both mass and chirality, which are usually called massive chiral fermions,[43,44] different from the massless Dirac fermions in graphene.[13–15]

When the SU(2) gauge potential is introduced, we can modify the tight-binding Hamiltonian (1) by Peierls substitution.[30,60,61] Subjected to a gauge field, the general Hamiltonian of particles reads as

$$H(\boldsymbol{r}, \boldsymbol{p} - q\boldsymbol{A}) = \frac{(\boldsymbol{p} - q\boldsymbol{A})^2}{2m} + V(\boldsymbol{r}), \tag{5}$$

which can be obtained by the momentum "translation transformation" from the original Hamiltonian,

$$H(\boldsymbol{r}, \boldsymbol{p} - q\boldsymbol{A}) = U^{\dagger}H(\boldsymbol{r}, \boldsymbol{p})U. \tag{6}$$

The unitary transform $U = {\rm e}^{-{\rm i}\frac{q}{\hbar}\int_{\boldsymbol{r}_0}^{\boldsymbol{r}}\boldsymbol{A}(\boldsymbol{r}')\cdot{\rm d}\boldsymbol{r}'}$. Then the eigenstates of the transformed Hamiltonian are $\phi'(\boldsymbol{r}) = U^{\dagger}\phi(\boldsymbol{r})$. As we know, the hopping integral of the tight-binding model is the overlapping integral of Wannier states, thus

$$\begin{aligned} t'_{ij} &= \int {\rm d}\boldsymbol{r}\phi'^{*}(\boldsymbol{r} - \boldsymbol{R}_i)H(\boldsymbol{r}, \boldsymbol{p} - q\boldsymbol{A})\phi'(\boldsymbol{r} - \boldsymbol{R}_j) \\ &= \int {\rm d}\boldsymbol{r}\,{\rm e}^{-{\rm i}\frac{q}{\hbar}\int_{\boldsymbol{R}_i}^{\boldsymbol{r}}\boldsymbol{A}(\boldsymbol{r}')\cdot{\rm d}\boldsymbol{r}'}\phi^{*}(\boldsymbol{r} - \boldsymbol{R}_i)H(\boldsymbol{r}, \boldsymbol{p} - q\boldsymbol{A}) \\ &\quad \times {\rm e}^{{\rm i}\frac{q}{\hbar}\int_{\boldsymbol{R}_j}^{\boldsymbol{r}}\boldsymbol{A}(\boldsymbol{r}')\cdot{\rm d}\boldsymbol{r}'}\phi(\boldsymbol{r} - \boldsymbol{R}_j) \\ &= \int {\rm d}\boldsymbol{r}\,{\rm e}^{-{\rm i}\frac{q}{\hbar}\int_{\boldsymbol{R}_i}^{\boldsymbol{r}}\boldsymbol{A}(\boldsymbol{r}')\cdot{\rm d}\boldsymbol{r}'}{\rm e}^{{\rm i}\frac{q}{\hbar}\int_{\boldsymbol{R}_j}^{\boldsymbol{r}}\boldsymbol{A}(\boldsymbol{r}')\cdot{\rm d}\boldsymbol{r}'} \\ &\quad \times \phi^{*}(\boldsymbol{r} - \boldsymbol{R}_i)H(\boldsymbol{r}, \boldsymbol{p})\phi(\boldsymbol{r} - \boldsymbol{R}_j) \\ &= {\rm e}^{{\rm i}\frac{q}{\hbar}\int_{\boldsymbol{R}_j}^{\boldsymbol{R}_i}\boldsymbol{A}(\boldsymbol{r})\cdot{\rm d}\boldsymbol{r}}t_{ij}, \end{aligned} \tag{7}$$

where

$$t_{ij} = \int {\rm d}\boldsymbol{r}\phi^{*}(\boldsymbol{r} - \boldsymbol{R}_i)H(\boldsymbol{r}, \boldsymbol{p})\phi(\boldsymbol{r} - \boldsymbol{R}_j).$$

Hence the tight-binding Hamiltonian with SU(2) gauge potential reads

$$H = -t\sum_{\langle ij\rangle\sigma\sigma' l} c^{\dagger}_{i\sigma l}T^{\sigma\sigma'}_{ij}c_{j\sigma' l} - t_{\perp}\sum_{i\sigma l} c^{\dagger}_{i\sigma l}c_{i\sigma(1-l)}, \tag{8}$$

where $T_{ij} = {\rm e}^{{\rm i}\frac{q}{\hbar}\int_{\boldsymbol{R}_j}^{\boldsymbol{R}_i}\boldsymbol{A}(\boldsymbol{r})\cdot{\rm d}\boldsymbol{r}}$. The artificial gauge field $\boldsymbol{A}$ can be produced by atom–laser interaction. Considering atoms with

4 internal states, 4 dressed states will occur in the presence of the laser field. The atoms are initially prepared in a degenerate subspace formed by the first 2 dressed states. When the transition to the states outside the subspace is forbidden, we can project the full Schrödinger equation onto the subspace and obtain the reduced Schrödinger equation $i\hbar\frac{\partial\Psi}{\partial t} = [\frac{(\boldsymbol{p}-\boldsymbol{A})^2}{2m} + V_{\text{eff}}]\Psi$.[26] Then the SU(2) artificial gauge field on neutral atoms is produced and can be tuned by the lasers. Following previous work on honeycomb lattice,[30,31] we choose a lattice translational invariant gauge. When the gauge is chosen appropriately, as shown in Fig. 2(a), $T_1 = \mathrm{e}^{\mathrm{i}\alpha\tau_x}$, $T_2 = \mathbb{1}_2$, $T_3 = \mathrm{e}^{\mathrm{i}\beta\tau_y}$, where $\tau_{x,y,z}$ are the Pauli matrices and α (β) are the gauge fluxes. Similarly, the Hamiltonian (8) with SU(2) gauge potential in the momentum space is described by

$$H(\boldsymbol{k}) = \begin{bmatrix} 0 & -tF(\boldsymbol{k}) & 0 & 0 \\ -tF^{\dagger}(\boldsymbol{k}) & 0 & -t_{\perp}\mathbb{1}_2 & 0 \\ 0 & -t_{\perp}\mathbb{1}_2 & 0 & -tF(\boldsymbol{k}) \\ 0 & 0 & -tF^{\dagger}(\boldsymbol{k}) & 0 \end{bmatrix}, \tag{9}$$

where $F(\boldsymbol{k}) = T_2 + \mathrm{e}^{\mathrm{i}\boldsymbol{k}\cdot\boldsymbol{a}_1}T_3^{\dagger} + \mathrm{e}^{\mathrm{i}\boldsymbol{k}\cdot\boldsymbol{a}_2}T_1^{\dagger}$.

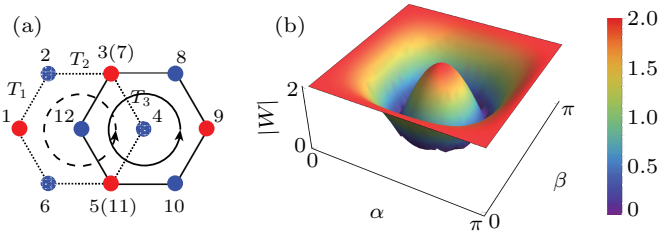


Fig. 2. (a) The illustration for the BHL subjected to the SU(2) gauge field. The odd (even) indices denote A (B) sites of the BHL. Subjected to SU(2) gauge field, the hopping integrals are dressed by $T_1 = \mathrm{e}^{\mathrm{i}\alpha\tau_x}$, $T_2 = \mathbb{1}$, $T_3 = \mathrm{e}^{\mathrm{i}\beta\tau_y}$. (b) The magnitude $|W|$ of the Wilson loop as a function of α and β in $[0,\pi]$ range. The Abelian regimes include the four edges of α–β square and the center point $(\pi/2,\pi/2)$, where $|W(\alpha,\beta)| = 2$.

The unitary transformation around a fundamental hexagon in Fig. 2(a) reads $T_{\hexagon} = T_3T_2T_1T_3^{\dagger}T_2^{\dagger}T_1^{\dagger}$. The Abelian and non-Abelian regimes can be distinguished by introducing Wilson loop $W = \mathrm{tr}T_{\hexagon}$,[28–31,36] which describes a gauge-invariant non-local quantity concerning the flux through the elementary plaquette. Only when the magnitude of the Wilson loop W equals to 2, will the loop transformation $T_{\hexagon}$ be trivial. If $|W| \neq 2$, the SU(2) gauge field is non-Abelian. For the plaquette in Fig. 2(a), $W = 2 - 4\sin^2\alpha\sin^2\beta$. As shown in Fig. 2(b), most regions of the α–β parameter space belong to non-Abelian regimes, other than four edges and the center point of the square.

3. Topological Lifshitz transition

For the graphene point $(\alpha,\beta) = (0,0)$, the Hamiltonian (9) is reduced to the Hamiltonian (2) with color degeneracy,

$$H(\boldsymbol{k}) = H_{\mathrm{t}}(\boldsymbol{k}) \otimes \mathbb{1}_2. \tag{10}$$

Therefore, the band structure at graphene point is the same with spectrum (3), except for the double degeneracy of each band [see Fig. 3(a)]. Consequently, the number of Dirac points increases from $N = 2$ to $N = 4$. Then we consider the entire Abelian regimes.

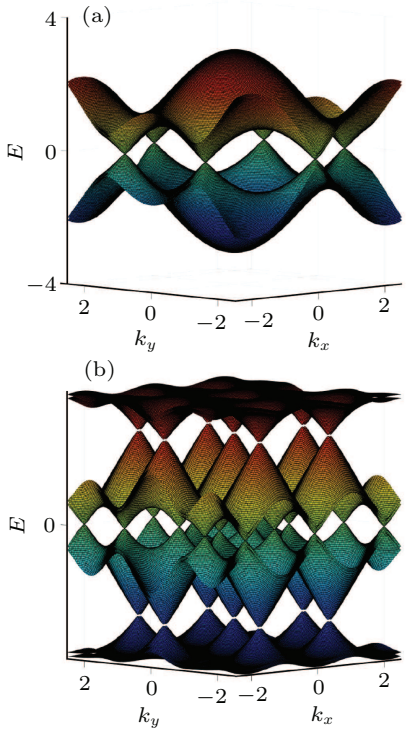


Fig. 3. Band structure of the BHL with SU(2) gauge potential for different fluxes (α,β). (a) Graphene point $\alpha = \beta = 0$. (b) π-flux point $\alpha = \beta = \pi/2$.

Comparing SU(2) gauge Hamiltonian (8) with Hamiltonian (1), we can easily find that the electron–hole symmetry persists against the gauge field. Thus, the spectrum modified by gauge potential is also symmetric around zero energy. Under these circumstances, all Dirac points can be identified by the zero energy modes of the uppermost valence band, which could be utilized to demonstrate the topologies of Fermi surfaces. Patterns of zero modes for different gauge fluxes (α,β) along the Abelian path $(0,0) \to (0,\pi) \to (\pi,\pi)$ are shown in Fig. 4. The number of Dirac points is invariant in the trivial Abelian regimes and only their positions are transported in the momentum space by the Abelian gauge field. The positions of Dirac points P_1 and P_2 in the trivial Abelian regimes are determined by the following expressions:

$$P_1 = \left(\frac{1}{3}(\alpha+\beta), \frac{1}{\sqrt{3}}\left(\alpha-\beta+\frac{4\pi}{3}\right)\right), \tag{11}$$

$$\mathrm{P}_2 = \left(-\frac{1}{3}(\alpha+\beta-2\pi), -\frac{1}{\sqrt{3}}\left(\alpha-\beta+\frac{2\pi}{3}\right)\right). \tag{12}$$

P_3 and P_4 are the space inversion of P_1 and P_2, respectively. If their coordinates exceed FBZ, these points must be translated into FBZ along reciprocal vectors.

Different from the trivial Abelian regimes in the four edges, the center point $(\alpha,\beta)=(\pi/2,\pi/2)$ is an Abelian π-flux point.[28–31] As shown in Fig. 3(b), the number of zero modes is doubled compared with previous Abelian phases [Fig. 3(a)]. The Dirac points locate at the following positions: $K=\frac{2\pi}{3}(1,\frac{1}{\sqrt{3}})$, $K'=\frac{2\pi}{3}(1,-\frac{1}{\sqrt{3}})$, $Q_1=\frac{2\pi}{3}(0,\frac{1}{\sqrt{3}})$, $Q_2=\frac{2\pi}{3}(0,-\frac{1}{\sqrt{3}})$, $Q_3=\frac{\pi}{3}(1,\frac{1}{\sqrt{3}})$, $Q_4=\frac{\pi}{3}(1,-\frac{1}{\sqrt{3}})$, $Q_5=-\frac{\pi}{3}(1,\frac{1}{\sqrt{3}})$ and $Q_6=-\frac{\pi}{3}(1,-\frac{1}{\sqrt{3}})$ [see Fig. 5(e)]. From above, we can conclude that the topology of Fermi surface at the π-flux point is not equivalent to those in trivial Abelian regimes. The different topologies of Fermi surfaces signify a topological Lifshitz transition[5] connecting the trivial Abelian regimes and the π-flux point, driven by the non-Abelian gauge potential.

To illustrate the topological Lifshitz transition, a topological argument must be attached. The universality class of gapless excitations is determined by a topological winding number.[5,30,66] If the Hamiltonian satisfy a particle–hole symmetry $\{\Gamma,H(\boldsymbol{k})\}=0$, where $\Gamma=\mathrm{diag}\{\mathbb{1}_2,-\mathbb{1}_2,\mathbb{1}_2,-\mathbb{1}_2\}$, we can define a local winding number

$$\nu=\frac{1}{4\pi\mathrm{i}}\oint_C \mathrm{tr}(\Gamma H^{-1}(\boldsymbol{k}))\mathrm{d}H(\boldsymbol{k}), \tag{13}$$

where C is a loop surrounding the singularity in the momentum space.[30,66] For the honeycomb lattice with SU(2) gauge potential, the topological charges of massless Dirac points are $\nu=\pm1$.[30] For trivial Abelian regimes on BHL, there are two negative topological charges $\nu(P_1)=\nu(P_2)=-2$, and two positive ones $\nu(P_3)=\nu(P_4)=+2$. For π-flux point, there are four positive topological charges $\nu(K',Q_2,Q_3,Q_6)=+2$ and four negative topological charges $\nu(K,Q_1,Q_4,Q_5)=-2$. In this way, the universality classes of trivial Abelian regimes and π-flux point are different, indicating a topological Lifshitz transition connecting these two phases driven by the non-Abelian gauge fluxes.[5]

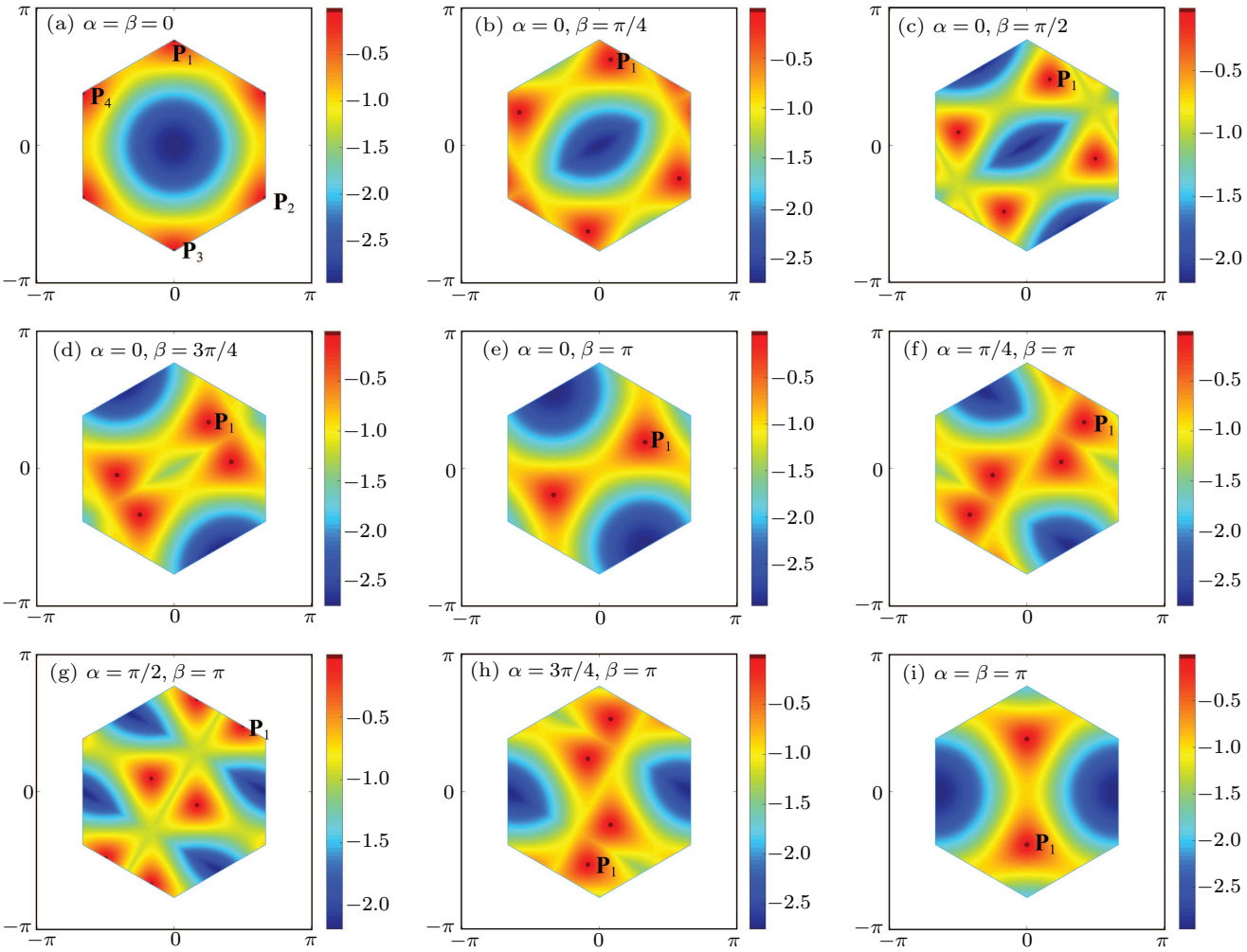


Fig. 4. Topologies of Fermi surfaces for different gauge fluxes (α,β) along the Abelian path $(0,0)\to(0,\pi)\to(\pi,\pi)$. In the trivial Abelian regimes, the number of Dirac points is invariant. The Abelian gauge field only changes the positions of these zero modes in momentum space. The position change of Dirac point P_1 with fluxes (α,β) is shown in detail.

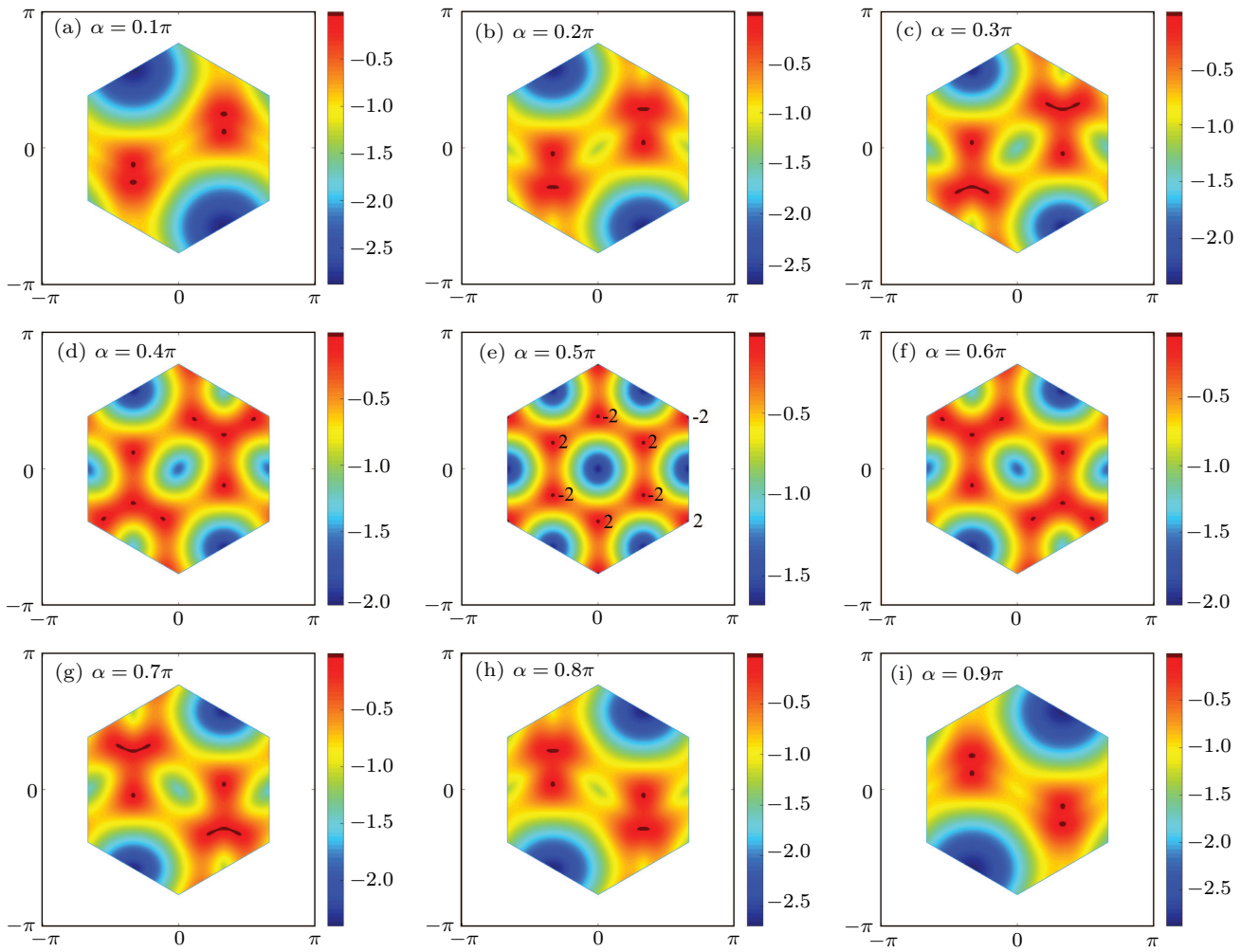


Fig. 5. Topology of Fermi surfaces for different gauge fluxes (α,β) along the non-Abelian path $(0,\pi)\to(\pi,0)$, where $\beta=\pi-\alpha$. There are four Dirac points in (a)–(b) and (h)–(i), which are the same with trivial Abelian regimes. Panels (c)–(g) belong to the $N=8$ phase.

4. Phase diagram

To investigate the topological Lifshitz transition thoroughly, we tune the gauge fluxes (α,β) along the non-Abelian path $(0,\pi)\to(\pi,0)$ and obtain the topologies of respective Fermi surfaces in Fig. 5. We find that the region around π-flux point is in the $N=8$ phase [Figs. 5(c)–5(g)]. It is necessary to obtain the phase boundary of the topological Lifshitz transition.

As we know, the energy bands can be obtained by solving the secular equation $\det[H(\boldsymbol{k})-E]=0$. If zero modes exist, the equation $\det[H(\boldsymbol{k})]=0$ will have roots, the number of which will equal the number of zero modes. Since the number of zero modes differs in the topological Lifshitz transition induced by non-Abelian SU(2) gauge potential, we can obtain the phase boundary by solving the equation $\det[H(\boldsymbol{k})]=0$. It is easy to find that

$$\det[H(\boldsymbol{k})]=t^8|\det[F(\boldsymbol{k})]|^4, \tag{14}$$

which is independent of t'. Thus the value of t' does not affect the phase transition. Therefore, the problem is reduced to solving the equation $\det[F(\boldsymbol{k})]=0$.

We substitute T_1, T_2 and T_3 in $F(\boldsymbol{k})=T_2+\mathrm{e}^{\mathrm{i}\boldsymbol{k}\cdot\boldsymbol{a}_1}T_3^\dagger+\mathrm{e}^{\mathrm{i}\boldsymbol{k}\cdot\boldsymbol{a}_2}T_1^\dagger$ and find

$$F(\boldsymbol{k})=\begin{bmatrix}F_{11}(\boldsymbol{k}) & F_{12}(\boldsymbol{k})\\ F_{21}(\boldsymbol{k}) & F_{22}(\boldsymbol{k})\end{bmatrix}, \tag{15}$$

where

$$\begin{aligned}
&F_{11}(\boldsymbol{k})=F_{22}(\boldsymbol{k})=1+\cos\beta\,\mathrm{e}^{\mathrm{i}\boldsymbol{k}\cdot\boldsymbol{a}_1}+\cos\alpha\,\mathrm{e}^{\mathrm{i}\boldsymbol{k}\cdot\boldsymbol{a}_2},\\
&F_{12}(\boldsymbol{k})=-\sin\beta\,\mathrm{e}^{\mathrm{i}\boldsymbol{k}\cdot\boldsymbol{a}_1}-\mathrm{i}\sin\alpha\,\mathrm{e}^{\mathrm{i}\boldsymbol{k}\cdot\boldsymbol{a}_2},\\
&F_{21}(\boldsymbol{k})=\sin\beta\,\mathrm{e}^{\mathrm{i}\boldsymbol{k}\cdot\boldsymbol{a}_1}-\mathrm{i}\sin\alpha\,\mathrm{e}^{\mathrm{i}\boldsymbol{k}\cdot\boldsymbol{a}_2}.
\end{aligned}$$

Thus,

$$\begin{aligned}
\det[F(\boldsymbol{k})] &= (1+\cos\beta\,\mathrm{e}^{\mathrm{i}\boldsymbol{k}\cdot\boldsymbol{a}_1}+\cos\alpha\,\mathrm{e}^{\mathrm{i}\boldsymbol{k}\cdot\boldsymbol{a}_2})^2\\
&\quad-[(\mathrm{i}\sin\alpha\,\mathrm{e}^{\mathrm{i}\boldsymbol{k}\cdot\boldsymbol{a}_2})^2-(\sin\beta\,\mathrm{e}^{\mathrm{i}\boldsymbol{k}\cdot\boldsymbol{a}_1})^2]\\
&= 1+\mathrm{e}^{2\mathrm{i}\boldsymbol{k}\cdot\boldsymbol{a}_1}+\mathrm{e}^{2\mathrm{i}\boldsymbol{k}\cdot\boldsymbol{a}_2}+2\cos\beta\,\mathrm{e}^{\mathrm{i}\boldsymbol{k}\cdot\boldsymbol{a}_1}\\
&\quad+2\cos\alpha\,\mathrm{e}^{\mathrm{i}\boldsymbol{k}\cdot\boldsymbol{a}_2}+2\cos\alpha\cos\beta\,\mathrm{e}^{\mathrm{i}\boldsymbol{k}\cdot(\boldsymbol{a}_1+\boldsymbol{a}_2)}.
\end{aligned} \tag{16}$$

To make $\det[F(\boldsymbol{k})]=0$, both the real and imaginary parts must equal zero, ie, $\mathrm{Re}[\det F(\boldsymbol{k})]=0$ and $\mathrm{Im}[\det F(\boldsymbol{k})]=0$. By eliminating variable k_x, the two equations can be reduced to a single equation with one variable $y=\cos(\sqrt{3}k_y)+$

$\cos\alpha\cos\beta$,

$$c_4 y^4 + c_3 y^3 + c_2 y^2 + c_1 y + c_0 = 0, \tag{17}$$

where

$$\begin{cases} c_4 = 16, \\ c_3 = -32\cos\alpha\cos\beta, \\ c_2 = 32\cos^2\alpha\cos^2\beta - 8, \\ c_1 = 8\cos\alpha\cos\beta[3 - 2(\cos^2\alpha + \cos^2\beta)], \\ c_0 = 1 - 4(\cos^2\alpha + \cos^2\beta) + 8\cos^2\alpha\cos^2\beta. \end{cases} \tag{18}$$

The number of roots in Eq. (17) can be determined by the discriminant

$$\Delta = \frac{1}{c_4}\det\begin{bmatrix} c_4 & c_3 & c_2 & c_1 & c_0 & 0 & 0 \\ 0 & c_4 & c_3 & c_2 & c_1 & c_0 & 0 \\ 0 & 0 & c_4 & c_3 & c_2 & c_1 & c_0 \\ 4c_4 & 3c_3 & 2c_2 & 1c_1 & 0 & 0 & 0 \\ 0 & 4c_4 & 3c_3 & 2c_2 & 1c_1 & 0 & 0 \\ 0 & 0 & 4c_4 & 3c_3 & 2c_2 & 1c_1 & 0 \\ 0 & 0 & 0 & 4c_4 & 3c_3 & 2c_2 & 1c_1 \end{bmatrix}. \tag{19}$$

When the discriminant $\Delta = 0$, the corresponding equation has multiple roots. Consequently, we obtain the phase diagram of gauge fluxes (α, β) in Fig. 6. The phase boundary of the topological Lifshitz transition is the red line, which corresponds to $\Delta = 0$. The $N = 4$ phase is outside the phase boundary, while $N = 8$ phase inside the boundary. The phase diagram can also be confirmed by calculating the Fermi surfaces.

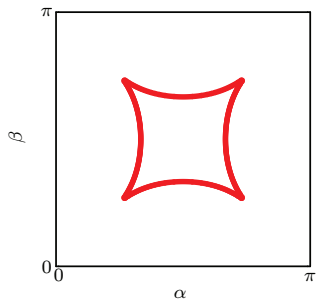


Fig. 6. The α–β phase diagram. The phase boundary of the topological Lifshitz transition is the red line, which corresponds to $\Delta = 0$. There are $N = 4$ Dirac points outside the boundary.

5. Novel edge states

Different from honeycomb lattice, there are some unique phenomena on the BHL, which also exhibit exotic changes under the influence of SU(2) gauge field. Localized edge states have been reported to exist at the zigzag edges of bilayer graphene.[67] Now we begin to investigate the effects of the SU(2) gauge potential on the localized edge states. A tunable band gap has been realized by applying a biased electric field on bilayer graphene.[45–49] Hence we consider the biased BHL nanoribbon with zigzag edges [see Fig. 1(b)]. When a gated voltage is applied to BHL, the Hamiltonian (9) should be modified by adding a term $H_V = V\,\mathrm{diag}\{\mathbb{1}_4, -\mathbb{1}_4\}$, where $2V$ is the voltage difference between the two layers. A two-photon dressing field can be used to produce an effective gauge potential for neutral atoms. Through the time dependence of the effective potential, we can generate synthetic electric field on neutral atoms.[25] A generalization of Bragg spectroscopy can be used to detect edge states in optical lattices.[68]

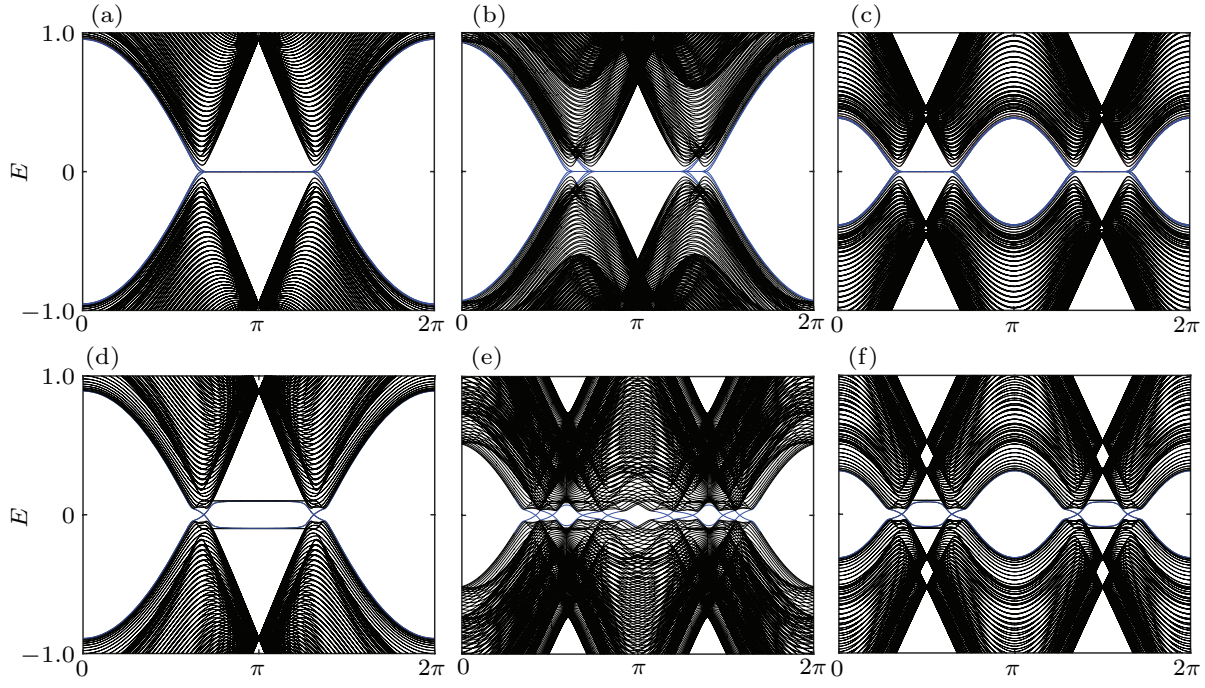


Fig. 7. Energy spectrum for a bilayer ribbon of $N_L = 80$ cells with zigzag edges. (a) $V = 0, \alpha = \beta = 0$. (b) $V = 0, \alpha = \beta = \pi/10$. (c) $V = 0, \alpha = \beta = \pi/2$. (d) $V = 0.1, \alpha = \beta = 0$. (e) $V = 0.1, \alpha = \beta = 2\pi/5$. (f) $V = 0.1, \alpha = \beta = \pi/2$.

When $V = 0$, we tune the gauge fluxes (α, β) along $(0,0) \to (\pi/2, \pi/2)$. Four partly flat bands at Fermi level locate in the range of $[2\pi/3, 4\pi/3]$ [Fig. 7(a)], which correspond to four edge states.[67] As we know, these bands are doubly degenerate and the increasing flux will result in a nondegeneracy. We can find that four additional dispersive bands appear away from the flat bands in Fig. 7(b). The nondegenerate flat bands are also transported by gauge fluxes in momentum space and thus their range is also enlarged. When the fluxes continue to increase, the nondegenerate flat bands will separate into two parts. Finally, for $\alpha = \beta = \pi/2$, the nondegeneracy disappears again, but the two parts of flat bands remain in Fig. 7(c).

Considering biased voltage $V = 0.1$, we show the energy spectrum of a bilayer ribbon for different gauge fluxes in Figs. 7(d)–7(f). The bias will move two flat bands from Fermi level to $E = \pm V$, and the other two edge states become two dispersive bands crossing the opened gap [Fig. 7(d)]. Similar to the unbiased case, the SU(2) gauge potential will destroy the color degeneracy and transport the bands. As a result, we can see eight band crossing in the gap when $\alpha = \beta = 2\pi/5$ in Fig. 7(e). At π-flux point, both the flat and crossing bands separate into two parts [Fig. 7(f)].

6. Summary

In this work, we systematically study the SU(2) gauge effects on BHL. Based on the tight-binding model of graphene bilayer, we deduce the model by Peierls substitution. A topological Lifshitz transition induced by the non-Abelian gauge potential is discovered. Topological Lifshitz transitions are identified by the topologies of Fermi surfaces. The Fermi surface at π-flux point consists of $N = 8$ Dirac points, instead of $N = 4$ in the trivial Abelian regimes. We also define a local winding number to classify the universality class of different topological phases. Then the phase diagram of gauge fluxes is demonstrated. The influence of gauge potential on edge states of biased bilayer ribbon is investigated. At the end, we would like to emphasize that the gauge potentials of different layers are independent in the present work, and the interlayer gauge fields cannot be considered. If we consider the interlayer gauge fields, the problem would become much more sophisticated and interesting, which will be studied in the future. In conclusion, our work will contribute to the research of topological Lifshitz transition and SU(2) gauge effects on bilayer honeycomb lattice. And the comprehension will be helpful for the electronic applications of bilayer graphene.

Acknowledgements

We are grateful to X. D. Zhang, F. Sun, D. Y. Jing, and J. K. Wang for helpful discussions.

This work was supported by the National Key R&D Program of China (Grant Nos. 2021YFA1400900, 2021YFA0718300, and 2021YFA1400243) and the National Natural Science Foundation of China (Grant No. 61835013).

References

[1] Hasan M Z and Kane C L 2010 *Rev. Mod. Phys.* **82** 3045
[2] Qi X L and Zhang S C 2011 *Rev. Mod. Phys.* **83** 1057
[3] Chiu C K, Teo J C Y, Schnyder A P and Ryu S 2016 *Rev. Mod. Phys.* **88** 035005
[4] Volovik G E 2007 *Lect. Notes Phys.* **718** 31
[5] Volovik G E 2017 *Low Temp. Phys.* **43** 47
[6] Kotov V N, Uchoa B and Sushkov O P 2021 *Phys. Rev. B* **103** 045403
[7] Novoselov K S, Geim A K, Morozov S V, Jiang D, Katsnelson M I, Grigorieva I V, Dubonos S V and Firsov A A 2005 *Nature* **438** 197
[8] Lu L, Wang Z, Ye D, Ran L, Fu L, Joannopoulos J D and Soljačić M 2015 *Science* **349** 622
[9] Lv B Q, Weng H M, Fu B B, Wang X P, Miao H, Ma J, Richard P, Huang X C, Zhao L X, Chen G F, Fang Z, Dai X, Qian T and Ding H 2015 *Phys. Rev. X* **5** 031013
[10] Burkov A A, Hook M D and Balents L 2011 *Phys. Rev. B* **84** 235126
[11] Fang C, Chen Y, Kee H Y and Fu L 2015 *Phys. Rev. B* **92** 081201
[12] Novoselov K S, Geim A K, Morozov S V, Jiang D, Zhang Y, Dubonos S V, Grigorieva I V and Firsov A A 2004 *Science* **306** 666
[13] Castro Neto A H, Guinea F, Peres N M R, Novoselov K S and Geim A K 2009 *Rev. Mod. Phys.* **81** 109
[14] Abergel D S L, Apalkov V, Berashevich J, Ziegler K and Chakraborty T 2010 *Adv. Phys.* **59** 261
[15] McCann E and Koshino M 2013 *Rep. Prog. Phys.* **76** 056503
[16] Bloch I 2005 *Nat. Phys.* **1** 23
[17] Bloch I, Dalibard J and Zwerger W 2008 *Rev. Mod. Phys.* **80** 885
[18] Jördens R, Strohmaier N, Günter K, Moritz H and Esslinger T 2008 *Nature* **455** 204
[19] Schneider U, Hackermuller L, Will S, Best T, Bloch I, Costi T A, Helmes R W, Rasch D and Rosch A 2008 *Science* **322** 1520
[20] Koepsell J, Bourgund D, Sompet P, Hirthe S, Bohrdt A, Wang Y, Grusdt F, Demler E, Salomon G, Gross C and Bloch I 2021 *Science* **374** 82
[21] Yang B, Sun H, Ott R, Wang H Y, Zache T V, Halimeh J C, Yuan Z S, Hauke P and Pan J W 2020 *Nature* **587** 392
[22] Ruseckas J, Juzeliūnas G, Öhberg P and Fleischhauer M 2005 *Phys. Rev. Lett.* **95** 010404
[23] Lin Y J, Compton R, Perry A, Phillips W, Porto J and Spielman I 2009 *Phys. Rev. Lett.* **102** 130401
[24] Lin Y J, Compton R L, Jiménez-García K, Porto J V and Spielman I B 2009 *Nature* **462** 628
[25] Lin Y J, Compton R L, Jiménez-García K, Phillips W D, Porto J V and Spielman I B 2011 *Nat. Phys.* **7** 531
[26] Dalibard J, Gerbier F, Juzeliūnas G and Öhberg P 2011 *Rev. Mod. Phys.* **83** 1523
[27] Goldman N, Juzeliūnas G, Öhberg P and Spielman I B 2014 *Rep. Prog. Phys.* **77** 126401
[28] Goldman N, Kubasiak A, Bermudez A, Gaspard P, Lewenstein M and Martin-Delgado M A 2009 *Phys. Rev. Lett.* **103** 035301
[29] Goldman N, Kubasiak A, Gaspard P and Lewenstein M 2009 *Phys. Rev. A* **79** 023624
[30] Bermudez A, Goldman N, Kubasiak A, Lewenstein M and Martin-Delgado M A 2010 *New J. Phys.* **12** 033041
[31] Sun F, Yu X L, Ye J, Fan H and Liu W M 2013 *Sci. Rep.* **3** 2119
[32] Wu W, Chen Y H, Tao H S, Tong N H and Liu W M 2010 *Phys. Rev. B* **82** 245102
[33] Chen Y H, Wu W, Tao H S and Liu W M 2010 *Phys. Rev. A* **82** 043625
[34] Wu W, Rachel S, Liu W M and Le Hur K 2012 *Phys. Rev. B* **85** 205102
[35] Chen Y H, Tao H S, Yao D X and Liu W M 2012 *Phys. Rev. Lett.* **108** 246402
[36] Wang L and Fu L 2013 *Phys. Rev. A* **87** 053612
[37] Chen Y H, Li J and Ting C S 2013 *Phys. Rev. B* **88** 195130
[38] Lin H F, Chen Y H, Liu H D, Tao H S and Liu W M 2014 *Phys. Rev. A* **90** 053627
[39] San-Jose P, González J and Guinea F 2012 *Phys. Rev. Lett.* **108** 216802
[40] Li L, Hao N, Liu G, Bai Z, Li Z D, Chen S and Liu W M 2015 *Phys. Rev. A* **92** 063618
[41] Lepori L, Fulga I C, Trombettoni A and Burrello M 2016 *Phys. Rev. A* **94** 053633

[42] Huang B B and Wan S L 2011 *Chin. Phys. Lett.* **28** 060303
[43] McCann E and Fal'ko V I 2006 *Phys. Rev. Lett.* **96** 086805
[44] Geim A K 2009 *Science* **324** 1530
[45] Gold C, Knothe A, Kurzmann A, Garcia-Ruiz A, Watanabe K, Taniguchi T, Fal'ko V, Ensslin K and Ihn T 2021 *Phys. Rev. Lett.* **127** 046801
[46] Castro E V, Novoselov K S, Morozov S V, Peres N M R, dos Santos J M B L, Nilsson J, Guinea F, Geim A K and Neto A H C 2007 *Phys. Rev. Lett.* **99** 216802
[47] Zhang Y, Tang T T, Girit C, Hao Z, Martin M C, Zettl A, Crommie M F, Shen Y R and Wang F 2009 *Nature* **459** 820
[48] Wang T, Guo Q, Liu Y and Sheng K 2012 *Chin. Phys. B* **21** 067301
[49] Ulstrup S, Johannsen J C, Cilento F, Miwa J A, Crepaldi A, Zacchigna M, Cacho C, Chapman R, Springate E, Mammadov S, Fromm F, Raidel C, Seyller T, Parmigiani F, Grioni M, King P D C and Hofmann P 2014 *Phys. Rev. Lett.* **112** 257401
[50] Murray J M and Vafek O 2014 *Phys. Rev. B* **89** 205119
[51] Vafek O, Murray J M and Cvetkovic V 2014 *Phys. Rev. Lett.* **112** 147002
[52] Tao H S, Chen Y H, Lin H F, Liu H D and Liu W M 2014 *Sci. Rep.* **4** 5367
[53] Mishra A and Lee S 2019 *Phys. Rev. B* **100** 045146
[54] Sun J H and Tang H K 2018 *Chin. Phys. B* **27** 077502
[55] Zhao X M, Wu Y J, Chen C, Liang Y and Kou S P 2016 *Chin. Phys. B* **25** 117303
[56] Zhang H, Arlego M and Lamas C A 2014 *Phys. Rev. B* **89** 024403
[57] Owerre S A 2016 *Phys. Rev. B* **94** 094405
[58] Zhang H, Lamas C A, Arlego M and Brenig W 2016 *Phys. Rev. B* **93** 235150
[59] Li J, Fu H, Yin Z, Watanabe K, Taniguchi T and Zhu J 2019 *Phys. Rev. Lett.* **122** 097701
[60] Hofstadter D R 1976 *Phys. Rev. B* **14** 2239
[61] Graf M and Vogl P 1995 *Phys. Rev. B* **51** 4940
[62] Malard L M, Nilsson J, Elias D C, Brant J C, Plentz F, Alves E S, Castro Neto A H and Pimenta M A 2007 *Phys. Rev. B* **76** 201401
[63] Nilsson J, Castro Neto A H, Guinea F and Peres N M R 2008 *Phys. Rev. B* **78** 045405
[64] Li Z Q, Henriksen E A, Jiang Z, Hao Z, Martin M C, Kim P, Stormer H L and Basov D N 2009 *Phys. Rev. Lett.* **102** 037403
[65] Kuzmenko A B, Crassee I, van der Marel D, Blake P and Novoselov K S 2009 *Phys. Rev. B* **80** 165406
[66] Wen X and Zee A 1989 *Nucl. Phys. B* **316** 641
[67] Castro E V, Peres N M R, Lopes dos Santos J M B, Neto A H C and Guinea F 2008 *Phys. Rev. Lett.* **100** 026802
[68] Goldman N, Beugnon J and Gerbier F 2012 *Phys. Rev. Lett.* **108** 255303